Franck–Condon simulation of photoelectron spectroscopy of HNO− and DNO−: Including Duschinsky effects

ARTICLE *in* CHEMICAL PHYSICS · OCTOBER 2003

Impact Factor: 1.65 · DOI: 10.1016/S0301-0104(03)00389-6

4 AUTHORS, INCLUDING:

Xianglei Kong
Nankai University
38 PUBLICATIONS **611** CITATIONS

Available online at www.sciencedirect.com
SCIENCE DIRECT®
Chemical Physics 294 (2003) 85–94
Chemical Physics
www.elsevier.com/locate/chemphys

Franck–Condon simulation of photoelectron spectroscopy of HNO^- and DNO^-: including Duschinsky effects

Jun Liang, Xianglei Kong, Xianyi Zhang, Haiyang Li *

Laboratory of Environment Spectroscopy, Anhui Institute of Optics and Fine Mechanics, Chinese Academy of Sciences, P.O. Box 1125, Hefei 230031, PR China

Received 13 May 2003; accepted 24 July 2003

Abstract

A theoretical method to calculate multidimensional Franck–Condon factors including Duschinsky effects is described and used to simulate the photoelectron spectra of HNO^- and DNO^- radicals. Geometry optimization and harmonic vibrational frequency calculations have been performed on the $\tilde{X}\ ^1A'$ and $\tilde{a}\ ^3A''$ states of HNO/DNO and $\tilde{X}\ ^2A''$ state of HNO^-/DNO^-. The theoretical spectra obtained by employing B3LYP/6-311+G(2d,p) values are in excellent agreement with the observed ones. In addition, the equilibrium geometry parameters, $R(NO) = 0.1335 \pm 0.0005$ nm, $\angle(HNO) = 106.3° \pm 0.5°$, of the $\tilde{X}\ ^2A''$ state of HNO^-/DNO^- are derived by employing an iterative Franck–Condon analysis procedure in the spectral simulation.

Keywords: Franck–Condon factor; Duschinsky effect; Spectral simulation; Photoelectron spectra

1. Introduction

The relative intensities of vibronic bands in the electronic transitions of molecules are governed by Franck–Condon (FC) principle. Under the assumptions that Born–Oppenheimer approximation is valid and that the electronic transition moment varies only slowly with the internuclear distances, the probability of a vibronic transition is proportional to the square of the vibrational overlap integral between the initial and final states. These values are commonly known as Franck–Condon factors (FCF). To calculate the overlap integrals for polyatomic molecules, the normal modes of the final state have to be expressed in terms of the normal modes of the initial state. In this theoretical framework, the geometries and normal modes in both electronic states are all needed in order to calculate the relative intensity distribution of a vibronic transition. As a development of density functional theory (DFT) and ab initio techniques, geometries and normal modes of small to medium size molecules in different electronic states can now be calculated routinely. Based on these methods, numerous applications of FC calculations have been presented in the literature [1–13], and most of these studies just focus on the interpretation of experimentally known spectra. Because the geometry difference between two

* Corresponding author. Tel./fax: +86-551-559-1550.
E-mail address: hli@aiofm.ac.cn (H. Li).

0301-0104/$ - see front matter © 2003 Elsevier B.V. All rights reserved.
doi:10.1016/S0301-0104(03)00389-6

electronic states is a major factor that influences FC intensities, the simulation of vibronic spectra of polyatomic molecules can be regarded as a valuable test with respect to the quality of calculated geometries and as a starting point to obtain improved structures. In addition, spectral simulations of vibrational structure based on computed Franck–Condon factors could provide fingerprint type identification of an observed spectrum, in terms of both the carrier and the electronic states in the transition (see, for example [8,9], and references therein). Also, it has been demonstrated that spectral simulations can be very useful in establishing vibrational assignments in an electronic spectrum observed with complex vibrational structure [1–4,6,9,10]. Moreover, even if the electronic spectrum is not rotationally resolved, if the geometrical parameters of one of the electronic states is well established by, for example, microwave spectroscopic measurements, the geometrical parameters of the other state can be determined by estimating the geometry change between the states by the iterative Franck–Condon analysis (IFCA) method [1–4,6–13].

In this paper, the theoretical methods to calculate multidimensional Franck–Condon factors are described. Geometry optimization and harmonic vibrational frequency calculations were performed on the $\tilde{X}\ ^1A'$ and $\tilde{a}\ ^3A''$ states of HNO/DNO and $\tilde{X}\ ^2A''$ state of HNO^-/DNO^-. Franck–Condon analyses and spectral simulation were carried out on the first two photoelectron bands of HNO^-/DNO^- (i.e., $\tilde{X}\ ^1A'$–$\tilde{X}\ ^2A''$ and $\tilde{a}\ ^3A''$–$\tilde{X}\ ^2A''$ transitions) [14]. In addition, employing the iterative Franck–Condon analysis procedure in the spectral simulation, the equilibrium geometry of the $\tilde{X}\ ^2A''$ state of HNO^-/DNO^- is derived.

2. Theoretical method

Different methods [15–21] have been proposed to calculate multidimensional Franck–Condon integrals. We chose the multidimensional generating function method described by Sharp and Rosenstock [16] for the integrals. First, the Duschinsky effect, or mode mixing of the initial and final electronic states, is expressed as

$$\mathbf{Q}' = \mathbf{J}\mathbf{Q} + \mathbf{K}, \tag{1}$$

where the $\mathbf{Q}$ and $\mathbf{Q}'$ are the normal coordinates of the two electronic states, respectively, and the matrix $\mathbf{J}$ and column vector $\mathbf{K}$ define the linear transformation. To obtain the matrix $\mathbf{J}$ and vector $\mathbf{K}$ in Eq. (1), in terms of Cartesian coordinates displacements [22–24], the general linear transformation of an arbitrary distortion $\mathbf{X}$ can be written

$$\mathbf{X}' = \mathbf{Z}\mathbf{X} + \mathbf{R}, \tag{2}$$

where $\mathbf{X}$ and $\mathbf{X}'$ are distortions expressed as Cartesian displacements from the equilibrium geometries of the anion and neutral, respectively. $\mathbf{R} = \mathbf{Z}\mathbf{R}_{\mathbf{eq}} - \mathbf{R}'_{\mathbf{eq}}$ is the change in equilibrium geometry between the anion and the neutral in Cartesian coordinates centered on the molecular center of mass, and $\mathbf{Z}$ is a rotation matrix, which is a unit matrix for most molecules of $\mathbf{C_{2V}}$ or higher symmetry ($\mathbf{Z} = 1$). In a conventional normal-mode analysis, the Cartesian displacements, $\mathbf{X}$, are transformed to internal coordinates, $\mathbf{S}$, and then to normal coordinates, $\mathbf{Q}$, and vice versa, by the $\mathbf{B}$ and $\mathbf{L}$ matrices. That is $\mathbf{S} = \mathbf{B}\mathbf{X}$ and $\mathbf{S} = \mathbf{L}\mathbf{Q}$. The definitions of $\mathbf{B}$ and $\mathbf{L}$ are consistent with [16]. After several substitutions, the relation to relate $\mathbf{Q}$ to $\mathbf{Q}'$ is obtained as

$$\mathbf{Q}' = (\mathbf{L}'^{-1}\mathbf{B}')[\mathbf{Z}\mathbf{M}^{-1}(\mathbf{L}^{-1}\mathbf{B})^{\dagger}\mathbf{Q} + \mathbf{R}], \tag{3}$$

where the superscript "†" indicates the transpose of the matrix. Eq. (3), substituted back into Eq. (1) gives expressions for $\mathbf{J}$ and $\mathbf{K}$

$$\mathbf{J} = (\mathbf{L}'^{-1}\mathbf{B}')\mathbf{Z}\mathbf{M}^{-1}(\mathbf{L}^{-1}\mathbf{B})^{\dagger} \quad \text{and}$$
$$\mathbf{K} = (\mathbf{L}'^{-1}\mathbf{B}')\mathbf{R}. \tag{4}$$

Having carried out the vibrational analyses for both the initial and final electronic states to obtain $\mathbf{B}$, $\mathbf{L}$, $\mathbf{B}'$ and $\mathbf{L}'$, one can use Eq. (4) for a description of the Duschinsky effect that is valid even for large changes in geometry or force constants.

The Cartesian atom displacement matrix (**ADM**) is defined as [25]

$$\mathbf{ADM} \equiv \mathbf{M}^{-1}(\mathbf{L}^{-1}\mathbf{B})^{\dagger}, \tag{5}$$

which relates $\mathbf{Q}$ to $\mathbf{X}$. $\mathbf{M}$ is a diagonal matrix with the atomic masses on the diagonal.

For a molecule of N atoms, if we define a $3N \times 3N - 6$ matrix, **g98**, containing the normal-mode output from Gaussian 98 [26], and a $3N-$

$6 \times 3N - 6$ diagonal matrix, **V**, containing the reduced masses for each mode on the diagonal, then

$$\mathbf{ADM} = (\mathbf{g98})\mathbf{V}^{-1/2}, \tag{6}$$

which removes the reduced-mass weighting. Finally, using Eqs. (4)–(6), **J** and **K** in terms of the Gaussian 98 output for the two electronic states are given by

$$\mathbf{J} = [\mathbf{M}(\mathbf{g98}')\mathbf{V}'^{-1/2}]^{\dagger}\mathbf{Z}(\mathbf{g98})\mathbf{V}^{-1/2} \quad \text{and}$$

$$\mathbf{K} = [\mathbf{M}(\mathbf{g98}')\mathbf{V}'^{-1/2}]^{\dagger}\mathbf{R}, \tag{7}$$

where, as usual, unprimed and primed quantities refer to the initial state and the final state in the transition, respectively. Having then computed **J** and **K**, the FCFs are easily produced using the algebraic expressions below. Following Sharp and Rosenstock [16], the arrays **A**–**E** are defined in terms of the Duschinsky rotations arrays, **J** and **K**, and the harmonic frequencies. A diagonal matrix **Γ** has the harmonic frequencies as diagonal elements. If FCFs are computed for a vibrationally cold molecule, i.e., no hot bands, then only **C** and **D** are necessary:

$$\mathbf{A} = 2\mathbf{\Gamma}'^{1/2}\mathbf{J}[\mathbf{J}^{\dagger}\mathbf{\Gamma}'\mathbf{J} + \mathbf{\Gamma}]^{-1}\mathbf{J}^{\dagger}\mathbf{\Gamma}'^{1/2} - \mathbf{1}, \tag{8a}$$

$$\mathbf{B} = -2\mathbf{\Gamma}'^{1/2}[\mathbf{J}(\mathbf{J}^{\dagger}\mathbf{\Gamma}'\mathbf{J} + \mathbf{\Gamma})^{-1}\mathbf{J}^{\dagger}\mathbf{\Gamma}' - 1]\mathbf{K}, \tag{8b}$$

$$\mathbf{C} = 2\mathbf{\Gamma}^{1/2}[\mathbf{J}^{\dagger}\mathbf{\Gamma}'\mathbf{J} + \mathbf{\Gamma}]^{-1}\mathbf{\Gamma}'^{1/2} - \mathbf{1}, \tag{8c}$$

$$\mathbf{D} = -2\mathbf{\Gamma}^{1/2}(\mathbf{J}^{\dagger}\mathbf{\Gamma}'\mathbf{J}^{-1} + \mathbf{\Gamma})^{-1}\mathbf{J}^{\dagger}\mathbf{\Gamma}'\mathbf{K}, \tag{8d}$$

$$\mathbf{E} = 4\mathbf{\Gamma}^{1/2}[\mathbf{J}^{\dagger}\mathbf{\Gamma}'\mathbf{J} + \mathbf{\Gamma}]^{-1}\mathbf{J}^{\dagger}\mathbf{\Gamma}'^{1/2}. \tag{8e}$$

The more general algebraic expressions were given by Chen and Pei [25], with m quanta in mode i and n quanta in mode j. The FCFs are

$$\mathrm{FCF}(m,n) = \frac{m!n!}{2^{m+n}}\left[\sum_{p=0}^{\binom{m}{n}}\sum_{q=0}^{\left\{\frac{m-p}{2}\right\}}\sum_{r=0}^{\left\{\frac{n-p}{2}\right\}} \times \frac{2^p D_i^{m-2q-p} D_j^{n-2r-p} C_{ii}^q C_{jj}^r C_{ij}^p}{p!q!r!(m-2q-p)!(n-2r-p)!}\right]^2. \tag{9}$$

The limit for the outermost summation is the lesser of the two numbers, m and n. The bracketed expressions for the limits of the remaining two summations are taken to mean the greatest integer less than or equal to $(m-p)/2$ or $(n-p)/2$.

3. Computational details

Geometry optimization and harmonic vibrational frequency calculations were carried out on the $\tilde{\mathrm{X}}\ ^1\mathrm{A}'$ and $\tilde{\mathrm{a}}\ ^3\mathrm{A}''$ states of the neutral molecule HNO and DNO, and $\tilde{\mathrm{X}}\ ^2\mathrm{A}''$ state of the negative ion HNO^- and DNO^- at the B3LYP, QCISD, QCISD(T), CCSD and CCSD(T) levels with the 6-311+G(2d,p) basis sets. The B3LYP, QCISD, QCISD(T), CCSD and CCSD(T) calculations were performed employing the Gaussian 98 suite of programs [26].

FCF calculations on the $\tilde{\mathrm{X}}\ ^1\mathrm{A}'$–$\tilde{\mathrm{X}}\ ^2\mathrm{A}''$ and $\tilde{\mathrm{a}}\ ^3\mathrm{A}''$–$\tilde{\mathrm{X}}\ ^2\mathrm{A}''$ photodetachment were carried out, employing B3LYP/6-311+G(2d,p) force constants, initially (see later text), B3LYP/6-311+G(2d,p) geometry for the electronic ground state $\tilde{\mathrm{X}}\ ^2\mathrm{A}''$ of the HNO^- (and DNO^-), and experimental geometries and B3LYP/6-311+G(2d,p) geometries of the neutral HNO/DNO for the electronic state $\tilde{\mathrm{X}}\ ^1\mathrm{A}'$ and $\tilde{\mathrm{a}}\ ^3\mathrm{A}''$, respectively. The theoretical method used in the FCF calculations has been described in Section 2. Briefly, the harmonic oscillator model was employed and Duschinsky rotation was included in the FCF calculations. The computed FCFs were then used to simulate the vibrational structure of the $\tilde{\mathrm{X}}\ ^1\mathrm{A}'$–$\tilde{\mathrm{X}}\ ^2\mathrm{A}''$ and $\tilde{\mathrm{a}}\ ^3\mathrm{A}''$–$\tilde{\mathrm{X}}\ ^2\mathrm{A}''$ photodetachment spectra of HNO^-/DNO^-, employing a Gaussian line-shape and a full-width-at-half-maximum (FWHM) of 425 cm^{-1} for the $\tilde{\mathrm{X}}\ ^1\mathrm{A}'$–$\tilde{\mathrm{X}}\ ^2\mathrm{A}''$ detachment and FWHM of 380 cm^{-1} for the $\tilde{\mathrm{a}}\ ^3\mathrm{A}''$–$\tilde{\mathrm{X}}\ ^2\mathrm{A}''$ detachment, respectively.

In order to obtain a reasonable match between the simulated and observed spectra, the iterative Franck–Condon analysis procedure [25] was also carried out, where the ground state geometrical parameters of the HNO/DNO molecule were fixed to the experimental values for the $\tilde{\mathrm{X}}\ ^1\mathrm{A}'$–$\tilde{\mathrm{X}}\ ^2\mathrm{A}''$ photodetachment processes and the triplet state geometrical parameters of the HNO/DNO was

fixed to the B3LYP/6-311+G(2d,p) values for the $\tilde{a}\ ^3A''$–$\tilde{X}\ ^2A''$ photodetachment processes, respectively, while the ground state geometrical parameters of the HNO^-/DNO^- were varied systematically. Thus, the ground state geometrical parameters of the HNO^-/DNO^- were varied until a best match between the simulated and observed spectra was obtained.

4. Results and discussions

4.1. Geometry optimization and frequency calculations

The optimized geometric parameters and computed vibrational frequencies for the $\tilde{X}\ ^1A'$ and $\tilde{a}\ ^3A''$ states of HNO and DNO, and $\tilde{X}\ ^2A''$ state of HNO and DNO as obtained in this work are listed in Tables 1–4. The theoretical and/or experimental values available in the literatures are also included for comparison. The bending vibration is denoted as ω_2, according to the convention for triatomic molecules. The other vibrational modes are listed in decreasing order of size, which designates the H–N (and D–N) stretch as ω_1 and the N–O stretch as ω_3.

From Tables 1 and 2, for the $\tilde{X}\ ^1A'$ state of HNO and DNO, the computed bond lengths and angles obtained at different levels of calculation seems to be highly consistent. For $R(HN)/R(DN)$, $R(NO)$ and $\angle(HNO)/\angle(DNO)$, the largest deviations between calculated and experimental bond lengths and angles are less than 0.0007, 0.0012 nm

Table 1
Summary of some computed and experimental geometrical parameters and vibrational frequencies (cm^{-1}) of the $\tilde{X}\ ^1A'$ and $\tilde{a}\ ^3A''$ state of HNO obtained at different levels of calculation

	R(HN) (nm)	R(NO) (nm)	∠(HNO) (°)	ω_1 (H–N)	ω_2 (bend)	ω_3 (N–O)
$\tilde{X}\ ^1A'$						
B3LYP/6-311+G(2d,p)	0.10632	0.12003	108.749	2875.5	1566.7	1654.3
QCISD/6-311+G(2d,p)	0.10575	0.12095	108.364	2964.6	1572.0	1617.7
QCISD(T)/6-311+G(2d,p)	0.10605	0.12193	108.113	2918.5	1518.2	1574.5
CCSD/6-311+G(2d,p)	0.10560	0.12078	108.316	2987.0	1578.9	1633.4
CCSD(T)/6-311+G(2d,p)	0.10598	0.12186	108.125	2929.7	1522.5	1576.7
CCSD/TZ2P[a]	0.1050	0.1207	108.0	2993 (113)	1581 (15)	1631 (59)
CCSD(T)/TZ2P[a]	0.1054	0.1219	107.80	2936 (126)	1511 (17)	1583 (43)
CCSD(T)/cc-pVTZ[b]	0.10554	0.12144	107.86	2938.0	1540.6	1596.9
CCSD(T)/cc-pVQZ[b]	0.10535	0.12107	108.01	2954.2	1546.5	1603.8
CASSCF(CCI)/ANO[c]	0.1062	0.1221	107.5			
CASSCF(ICCI)/cc-pVTZ[d]	0.10533	0.12174	107.75	2623	1468	1540
Expt.	0.1063[e]	0.1212[e]	108.6[e]	2683.95[f]	1500.82[g]	1565.34[g]
$\tilde{a}\ ^3A''$						
B3LYP/6-311+G(2d,p)	0.10310	0.12253	119.382	3284.8	1066.2	1577.0
QCISD/6-311+G(2d,p)	0.10286	0.12333	118.161	3351.7	1046.9	1510.3
QCISD(T)/6-311+G(2d,p)	0.10314	0.12358	118.862	3314.0	1054.9	1523.4
CCSD/6-311+G(2d,p)	0.10282	0.12286	118.698	3363.7	1056.3	1561.0
CCSD(T)/6-311+G(2d,p)	0.10311	0.12336	118.997	3319.6	1050.9	1541.0
CASSCF(CCI)/ANO[c]	0.1014	0.1231	120.4			
CASSCF(ICCI)/cc-pVTZ[d]	0.1011	0.1239	116.969	3312	862	1514
Expt.					992 (150)[h]	1468 (140)[h]

[a] Ref. [27].
[b] Ref. [28].
[c] Ref. [29].
[d] Ref. [30].
[e] Ref. [31].
[f] Ref. [32].
[g] Ref. [33].
[h] Ref. [14].

Table 2
Summary of some computed and experimental geometrical parameters and vibrational frequencies (cm^{-1}) of the $\tilde{X}\ ^1A'$ and $\tilde{a}\ ^3A''$ state of DNO obtained at different levels of calculation

	R(DN) (nm)	R(NO) (nm)	∠(DNO) (°)	ω_1 (D–N)	ω_2 (bend)	ω_3 (N–O)
$\tilde{X}\ ^1A'$						
B3LYP/6-311+G(2d,p)	0.10632	0.12003	108.749	2105.2	1187.7	1646.1
QCISD/6-311+G(2d, p)	0.10571	0.12093	108.382	2171.3	1193.2	1607.4
QCISD(T)/6-311+G(2d,p)	0.10607	0.12191	108.170	2133.4	1175.1	1533.2
CCSD/6-311+G(2d,p)	0.10560	0.12078	108.316	2184.5	1197.5	1624.2
CCSD(T)/6-311+G(2d,p)	0.10598	0.12186	108.125	2143.2	1176.6	1537.4
CCSD(T)/cc-pVQZ[a]	0.106875	0.121455	108.121	2161.3	1180.4	1583.2
Expt.	0.1063[b]	0.1212[b]	108.6[b]	2025.1[c]	1156[d]	1546.9[e]
$\tilde{a}\ ^3A''$						
B3LYP/6-311+G(2d,p)	0.10310	0.12253	119.382	2403.2	814.4	1561.6
QCISD/6-311+G(2d,p)	0.10286	0.12333	118.161	2455.1	801.1	1492.1
QCISD(T)/6-311+G(2d,p)	0.10302	0.12355	118.255	2429.0	807.4	1517.8
CCSD/6-311+G(2d,p)	0.10284	0.12285	118.676	2459.8	808.1	1543.6
CCSD(T)/6-311+G(2d,p)	0.10311	0.12337	118.997	2429.2	802.7	1524.2
Expt.					750 (140)[e]	1452 (140)[e]

[a] Ref. [28].
[b] Ref. [31].
[c] Ref. [33].
[d] Ref. [34].
[e] Ref. [14].

Table 3
Summary of some computed and experimental geometrical parameters and vibrational frequencies (cm^{-1}) of the $\tilde{X}\ ^2A''$ state of HNO^- obtained at different levels of calculation

	R(HN) (nm)	R(NO) (nm)	∠(HNO) (°)	ω_1 (H–N)	ω_2 (bend)	ω_3 (N–O)
B3LYP/6-311+G(2d,p)	0.10533	0.13328	106.199	2869.6	1425.0	1150.6
QCISD/6-311+G(2d,p)	0.10496	0.133900	105.8139	2955.8	1427.5	1152.6
QCISD(T)/6-311+G(2d,p)	0.10536	0.13479	105.606	2898.9	1405.7	1110.2
CCSD/6-311+G(2d,p)	0.10490	0.13364	105.792	2970.6	1436.6	1174.4
CCSD(T)/6-311+G(2d,p)	0.10534	0.13466	105.6597	2903.9	1409.0	1118.4
MP2/6-311+G*[a]	0.10447	0.13327	106.178	3029	1474	1183
MP4/6-311+G*[a]	0.10545	0.13421	106.040			
QCISD/6-311+G*[a]				2909	1462	1180
Expt.				2750.8[b]		1153.0[c]

[a] Ref. [35].
[b] Ref. [36].
[c] Ref. [14].

and 0.5°, respectively (see Table 1). The estimated values based on density functional theory at the B3LYP/6-311+G(2d,p) level, are 0.10632, 0.12003 nm and 108.749°. The differences between calculated and experimental values are only 0.00002, 0.0012 nm and 0.15° for R(HN)/R(DN), R(NO) and ∠(HNO)/∠(DNO), respectively. Both the optimized geometric parameters and the vibrational frequencies calculated at B3LYP/6-311+G(2d,p) level gave the best agreement with the corresponding available experimental values, and were therefore utilized in subsequent FC analyses and spectral simulation.

For the $\tilde{a}\ ^3A''$ state of HNO/DNO, the computed bond lengths R(HN)/R(DN) and R(NO) obtained by different theoretical methods are seen to be highly consistent. However, the computed bond angle of the $\tilde{a}\ ^3A''$ state appears to be more sensitive

Table 4
Summary of some computed and experimental geometrical parameters and vibrational frequencies (cm^{-1}) of the $\tilde{X}\ ^2A''$ state of DNO^- obtained at different levels of calculation

	R(DN) (nm)	R(NO) (nm)	∠(DNO) (°)	ω_1 (D–N)	ω_2 (bend)	ω_3 (N–O)
B3LYP/6-311+G(2d,p)	0.10532	0.13321	106.262	2099.9	1050.4	1169.5
QCISD/6-311+G(2d,p)	0.10496	0.13385	105.8887	2162.2	1058.3	1163.4
QCISD(T)/6-311+G(2d,p)	0.10536	0.13479	105.606	2121.7	1035.5	1125.9
CCSD/6-311+G(2d,p)	0.10489	0.13365	105.777	2173.7	1064.5	1184.0
CCSD(T)/6-311+G(2d,p)	0.10531	0.13467	105.596	2127.9	1038.4	1133.4
Expt.						1113.0[a]

[a] Ref. [14].

to the levels of calculation. From Tables 1 and 2, it can be seen that the computed angles converge towards smaller values when the level of calculation is improved from B3LYP/6-311+G(2d,p) to QCISD/6-311+G(2d,p) or CCSD/6-311+G(2d,p). This shows the effects of higher-order electron correlation on the computed bond angle of the $\tilde{a}\ ^3A''$ state of HNO/DNO. For the $\tilde{a}\ ^3A''$ state of HNO/DNO, because no experimental geometric values are available for comparison, it is expected that the geometrical parameters obtained at the higher levels of calculation should be the more reliable. Regarding the computed vibrational frequencies, for the $\tilde{a}\ ^3A''$ state of HNO/DNO, the values obtained at the various levels are reasonably consistent, especially with respect to the stretching H–N mode ω_1 (see Table 1). The biggest frequency difference between B3LYP/6-311+G (2d,p) and CCSD/6-311+G(2d,p) is 78.9 cm^{-1} for the stretching H–N mode ω_1. The B3LYP/6-311+G(2d,p) results give the best overall agreement to the corresponding available experimental values (see Tables 1 and 2, respectively), and were therefore utilized in subsequent FC analyses and spectral simulations.

From Tables 3 and 4, for the $\tilde{X}\ ^2A''$ state of HNO^- and DNO^-, it seems that the computed bond lengths R(HN)/R(DN) and R(NO) at different levels of calculation are generally consistent. The computed bond angles of the $\tilde{X}\ ^2A''$ state, as in the $\tilde{a}\ ^3A''$ states of HNO/DNO, appears to be more sensitive to the levels of calculation. The calculated geometry of HNO^-/DNO^- remains to be tested, since there is no complete experimental information yet on the structure of this system. In our present work, the more reliable bond length R(NO) and bond angle ∠(HNO)/∠(DNO) are obtained by the iterative Franck–Condon analysis. The vibrational frequencies obtained at the B3LYP/6-311+G(2d,p) level of theory are the best agreement with the experimental values. Hence, these values were employed in spectral simulation.

4.2. Franck–Condon simulations

4.2.1. $\tilde{X}\ ^1A'$–$\tilde{X}\ ^2A''$ detachment

For $\tilde{X}\ ^1A'$–$\tilde{X}\ ^2A''$ detachment, the simulated photoelectron spectra of HNO^- and DNO^- are shown in Figs. 1(b) and 2(b), respectively, with the experimental observed photoelectron spectra shown in Figs. 1(a) and 2(a). Vibrational assignments for the stretching mode ω_3 of the neutral molecule HNO and DNO are also provided, respectively, with the label $(0,0,n-0,0,0)$ corresponding to $(0,0,\omega_3-0,0,0)$ transition (see Figs. 1(b) and 2(b), respectively). The computed FCFs for the H–N/D–N stretching ω_1 and the H–N–O/D–N–O bending ω_2 modes were found to be negligibly small, therefore the ω_1 and ω_2 mode are not included in the assignment. In spectral simulation, a FWHM of 425 cm^{-1} was utilized with Gaussian band envelopes for HNO/DNO. This quantity is equal to that of the corresponding experimental spectra. The relative intensities were chosen to match the first vibronic profile between 1.5 and 2.5 eV in the experimental spectra [14].

It was found that the computed photoelectron spectra of HNO^- and DNO^- for $\tilde{X}\ ^1A'$–$\tilde{X}\ ^2A''$ detachment are almost identical to the experimental spectra. This suggests that for the ground electronic state of HNO and DNO, the computed geometry changes upon detachment at the B3LYP/6-311+G(2d,p) level are highly accurate, and the

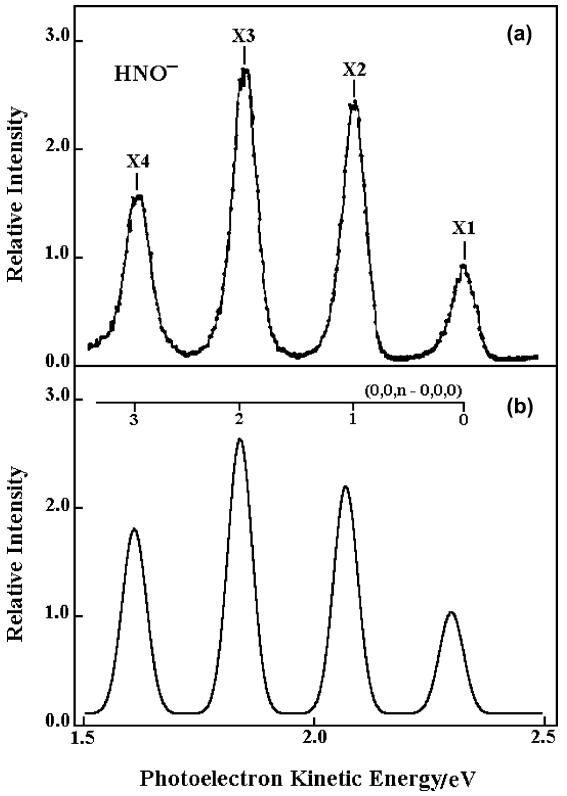

Fig. 1. (a) The experimental photoelectron spectrum of HNO^- (from [14]) and (b) the simulated spectrum with vibrational assignments provided for the $\tilde{X}\ ^1A'$–$\tilde{X}\ ^2A''$ detachment process. The FWHM used for the components of the simulated spectra is 425 cm^{-1}.

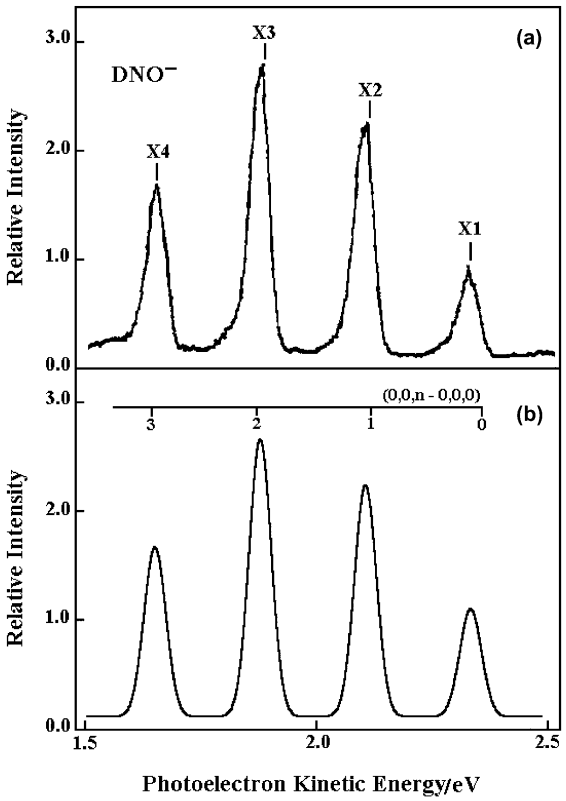

Fig. 2. (a) The experimental photoelectron spectrum of DNO^- (from [14]) and (b) the simulated spectrum with vibrational assignments provided for the $\tilde{X}\ ^1A'$–$\tilde{X}\ ^2A''$ detachment process. The FWHM used for the components of the simulated spectra is 425 cm^{-1}.

harmonic model seems to be reasonably adequate in this case.

The variations of geometries of the molecules between the electronic states using the iterative FC analysis (IFCA) method [1–4,6–13] would yield better matches between the simulated and observed spectra than that obtained with the B3LYP/6-311+G(2d,p) geometries. A reasonably reliable bond length of R(NO) for the ground state $\tilde{X}\ ^2A''$ of HNO^-/DNO^- can be deduced based on the experimental structural parameters of HNO/DNO in the $\tilde{X}\ ^1A'$ state and the computed geometry changes upon photodetachment at the B3LYP/6-311+G(2d,p) level. For $\tilde{X}\ ^2A''$–$\tilde{X}\ ^1A'$ photodetachment spectrum, the latter values were shown to be reliable from the excellent agreement between the simulated and observed spectra as mentioned above. Hence, by using the iterative Franck–Condon analysis method, the best IFCA bond length R(NO) obtained for the $\tilde{X}\ ^2A''$ state of HNO^-/DNO^-, employing the B3LYP/6-311+G(2d,p) force constants, is 0.1335 ± 0.0005 nm.

4.2.2. $\tilde{a}\ ^3A''$–$\tilde{X}^2A''$ detachment

For $\tilde{a}\ ^3A''$–$\tilde{X}\ ^2A''$ photodetachment, the simulated photoelectron spectra of HNO^- and DNO^- are shown in Figs. 3(b) and 4(b), respectively, with the experimental observed photoelectron spectra shown in Figs. 3(a) and 4(a). Vibrational assignments for the bending ω_2 and stretching modes ω_3 of the neutral molecule HNO/DNO are also

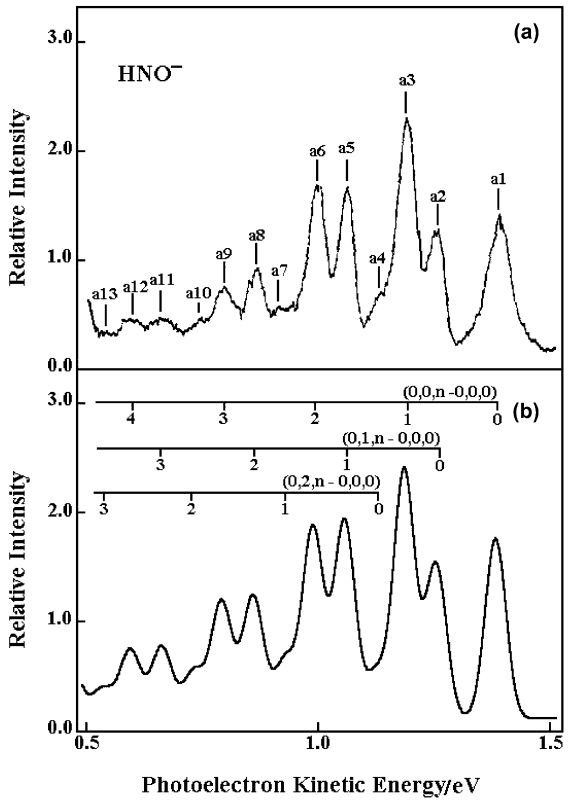

Fig. 3. (a) The experimental photoelectron spectrum of HNO^- (from [14]) and (b) the simulated spectrum with vibrational assignments provided for the $\tilde{a}\ ^3A''$–$\tilde{X}\ ^2A''$ detachment process. The FWHM used for the components of the simulated spectra is 380 cm^{-1}.

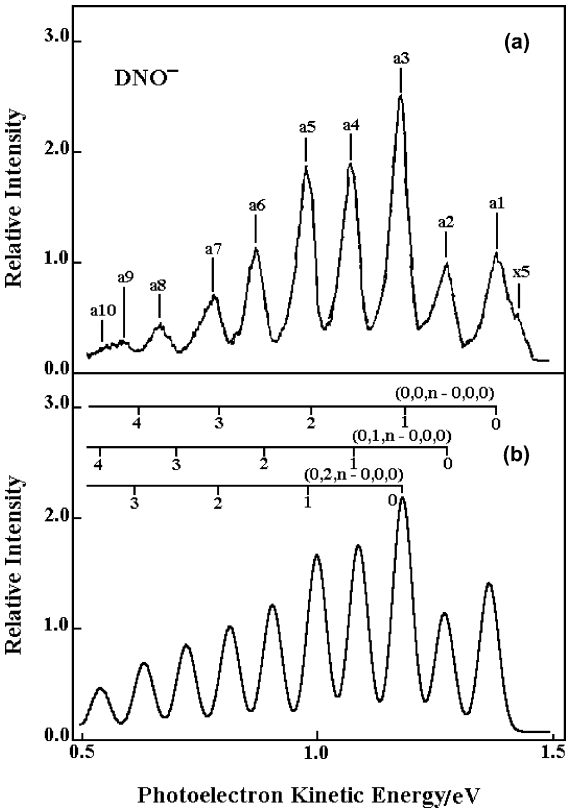

Fig. 4. (a) The experimental photoelectron spectrum of DNO^- (from [14]) and (b) the simulated spectrum with vibrational assignments provided for the $\tilde{a}\ ^3A''$–$\tilde{X}\ ^2A''$ detachment process. The FWHM used for the components of the simulated spectra is 380 cm^{-1}.

provided, respectively, with the label $(0,0,n-0,0,0)$, $(0,1,n-0,0,0)$ and $(0,2,n-0,0,0)$ corresponding to $(0, \omega_2, \omega_3 - 0,0,0)$ transition. The computed FCFs for the ω_1 mode were found to be negligibly small and therefore the ω_1 mode is not included in the assignments. In spectral simulation, a FWHM of 380 cm^{-1} was utilized with Gaussian band envelopes for HNO/DNO. This quantity is slightly lower than that of the corresponding experimental spectra (425 cm^{-1}). The relative intensities were chosen to match the second vibronic profile between 0.5 and 1.5 eV in the experimental spectra [14].

Comparing the simulated spectra in Figs. 3(b) and 4(b) and the experimental one in Figs. 3(a) and 4(a), respectively, it can been seen that reasonably good agreements are obtained mainly for the vibrational peaks with low quantum numbers, and the overall agreements of the intensity pattern are fair. Discrepancies between simulation and observation become larger for peaks with higher quantum numbers. This is mainly due to anharmonicity effects not included in the FCF calculation. With vibrational quantum numbers increasing, the stronger the anharmonicity effect is and the greater the influence on the simulated spectra. This is also true for other molecules, especially those containing a hydrogen atom [7,11].

By using the same IFCA method above, the best IFCA bond angle $\angle$(HNO)/$\angle$(DNO) obtained for the $\tilde{X}\ ^2A''$ state of HNO^-/DNO^-, employing the B3LYP/6-311+G(2d,p) geometries of the $\tilde{X}^1A'$

for HNO/DNO and IFCA bond length R(NO) obtained for the $\tilde{X}\ ^2A''$ state of HNO^-/DNO^- in this work and the B3LYP/6-311+G(2d,p) force constants, is $106.3° \pm 0.5°$.

It should be noted that since no H–N/D–N stretching structure (i.e., structure in ω_1), is observed in the first and second profiles (in the experimental spectra of [14]) for both states of interest, the computed R(HN)/R(DN) bond length change from the B3LYP calculations was assumed in the IFCA procedure. In view of the near-perfect match between the best-simulated spectrum and the observed spectrum, we anticipate the B3LYP R(HN)/R(DN) change to be close to the real one.

5. Conclusion

In the present study, attempts have been made to simulate the observed $\tilde{X}\ ^1A'$–$\tilde{X}\ ^2A''$ and $\tilde{a}\ ^3A''$–$\tilde{X}\ ^2A''$ detachment photoelectron spectra of HNO^-/DNO^-, using a harmonic model and including Duschinsky effects. In the case of the photoelectron spectra of the $\tilde{X}\ ^1A'$–$\tilde{X}\ ^2A''$ detachments, it seems that the harmonic model is reasonably adequate. A rather reliable bond length R(NO) of HNO^-/DNO^- was obtained for the first time, through the IFCA procedure. Based on the sensitivity of the relative intensities towards the variation of the bond length, the uncertainty in the R(NO) distance is probably around ± 0.0005 nm. For the $\tilde{a}\ ^3A''$–$\tilde{X}\ ^2A''$ detachment, it is clear that the harmonic model is inadequate. Nevertheless, focusing only on the relative intensities of the vibrational peaks with lower state quantum numbers, the FC simulated spectrum is reasonably consistent with the experimental spectrum. Since a perfect match between simulation and the whole spectra for the $\tilde{a}\ ^3A''$–$\tilde{X}\ ^2A''$ detachment process is not possible, the uncertainties in the IFCA geometric parameters obtained for the $\tilde{X}\ ^2A''$ state of HNO^- (and DNO^-) could not be reliably established. Clearly, anharmonicity should be incorporated into the model for computing FCFs in order to achieve better agreement between simulation and observation and hence obtain a more reliable IFCA geometry. Franck–Condon factor calculations that consider anharmonicity effects will be our future work.

Acknowledgements

This work is supported by the National Natural Science Foundation of China (No. 20073042).

References

[1] E.P.F. Lee, D.K.W. Mok, J.M. Dyke, F.T. Chau, J. Phys. Chem. A 106 (2002) 10130.
[2] F.T. Chau, J.M. Dyke, E.P.F. Lee, D.K.W. Mok, J. Chem. Phys. 115 (2001) 5816.
[3] D.C. Wang, F.T. Chau, D.K.W. Mok, E.P.F. Lee, L. Beeching, J.S. Ogden, J.M. Dyke, J. Chem. Phys. 114 (2001) 10682.
[4] E.P.F. Lee, J.M. Dyke, D.K.W. Mok, R.P. Claridge, F.T. Chau, J. Phys. Chem. A 105 (2001) 9533.
[5] S. Schumm, M. Gerhards, K. Kleinermanns, J. Phys. Chem. A 104 (2000) 10648.
[6] D.K.W. Mok, E.P.F. Lee, F.T. Chau, D.C. Wang, J.M. Dyke, J. Chem. Phys. 113 (2000) 5791.
[7] E.P.F. Lee, D.K.W. Mok, J.M. Dyke, F.T. Chau, Chem. Phys. Lett. 340 (2001) 348.
[8] F.T. Chau, E.P.F. Lee, D.K.W. Mok, D.C. Wang, J.M. Dyke, J. Electron Spectrosc. Relat. Phenom. 108 (2000) 75.
[9] J.M. Dyke, S.D. Gamblin, N. Hooper, E.P.F. Lee, A. Morris, D.K.W. Mok, F.T. Chau, J. Chem. Phys. 112 (2000) 6262.
[10] F.T. Chau, D.C. Wang, E.P.F. Lee, J.M. Dyke, D.K.W. Mok, J. Phys. Chem. A 103 (1999) 4925.
[11] F.T. Chau, J.M. Dyke, E.P.F. Lee, D.C. Wang, J. Electron Spectrosc. Relat. Phenom. 97 (1998) 33.
[12] F.T. Chau, E.P.F. Lee, D.C. Wang, J. Phys. Chem. A 101 (1997) 1603.
[13] F.T. Chau, J.M. Dyke, E.P.F. Lee, A. Ridha, D.C. Wang, Chem. Phys. 224 (1997) 157.
[14] H.B. Ellis, G.B. Ellison, J. Chem. Phys. 78 (1983) 6541.
[15] J.B. Coon, R.E. Dewames, C.M. Loyd, J. Mol. Spectrosc. 8 (1962) 285.
[16] T.E. Sharp, H.M. Rosenstock, J. Chem. Phys. 41 (1964) 3453.
[17] H. Kupka, P.H. Cribb, J. Chem. Phys. 85 (1986) 1303.
[18] E.V. Doktorov, I.A. Malkin, V.I. Manko, J. Mol. Spectrosc. 56 (1975) 1.
[19] E.V. Doktorov, I.A. Malkin, V.I. Manko, J. Mol. Spectrosc. 64 (1977) 302.
[20] T.R. Faulkner, F.S. Richardson, J. Chem. Phys. 70 (1979) 1201.
[21] K.M. Chen, C.C. Pei, Chem. Phys. Lett. 165 (1990) 532.
[22] A. Warshel, J. Chem. Phys. 62 (1975) 214.
[23] A. Warshel, M. Karplus, Chem. Phys. Lett. 17 (1972) 7.

[24] A. Warshel, M. Karplus, J. Am. Chem. Soc. 96 (1974) 5677.
[25] P. Chen, Photoelectron spectroscopy of reactive intermediates, in: C.Y. Ng, T. Baer, I. Powis (Eds.), Unimolecular and Bimolecular Reaction Dynamics, Wiley, New York, 1994, p. 371.
[26] M.J. Frisch, G.W. Trucks, H.B. Schlegel, G.E. Scuseria, M.A. Robb, J.R. Cheeseman, V.G. Zakrzewski, J.A. Montgomery, R.E. Stratmann, J.C. Burant, S. Dapprich, J.M. Millam, A.D. Daniels, K.N. Kudin, M.C. Strain, O. Farks, J. Tomasi, V. Barone, M. Cossi, R. Cammi, B. Mennucci, C. Pomelli, C. Adamo, S. Cliffoird, J. Ochterski, G.A. Petersson, P.Y. Ayala, Q. Cui, K. Morokuma, D.K. Malick, A.D. Rabuck, K. Raghavachari, J.B. Foresman, J. Cioslowski, J.V. Ortiz, B.B. Stefanov, G. Liu, A. Liashenko, P. Piskorz, I. Komaromi, R. Gomperts, R.L. Martin, D.J. Fox, T. Keith, M.A. Al-Laham, C.Y. Peng, A. Nanayakkara, C. Gonzalez, M. Challacombem, P.M.W. Gill, B.G. Johnson, W. Chen, M.W. Wong, J.L. Andres, M. Head-Gordon, E.S. Replogle, J.A. Pople, Gaussian 98, Gaussian, Inc., Pittsburgh, PA, 1998.
[27] T.J. Lee, J. Chem. Phys. 99 (1993) 9783.
[28] C.E. Dateo, T.J. Lee, D.W. Schwenke, J. Chem. Phys. 101 (1994) 5853.
[29] S.P. Walch, C.M. Rohlfing, J. Chem. Phys. 91 (1989) 2939 .
[30] R. Guadagrini, G.C. Schatz, S.P. Walch, J. Chem. Phys. 102 (1995) 774.
[31] M.D. Harmony, V.W. Laurie, R.L. Kuczkowski, R.H. Schwendeman, D.A. Ramsay, F.J. Lovas, W.J. Lafferty, A.G. Maki, J. Phys. Chem. Ref. Data 8 (1979) 619.
[32] J.W.C. Johns, A.R.W. McKellar, E. Weinberger, Can. J. Phys. 61 (1983) 1106.
[33] J.W.C. Johns, A.R.W. McKellar, J. Chem. Phys. 66 (1977) 1217.
[34] M.E. Jacox, D.E. Milligan, J. Mol. Spectrosc. 48 (1973) 536.
[35] K.A. Robins, J.W. Farley, J.L. Toto, J. Chem. Phys. 99 (1993) 9770.
[36] H.B. Miller, J.L. Hardwick, J.W. Farley, J. Mol. Spectrosc. 134 (1989) 329.